RESEARCH PAPER

Single-step replicable microfluidic check valve for rectifying and sensing low Reynolds number flow

J. Loverich · I. Kanno · H. Kotera

Abstract This paper presents a new microfluidic check valve well suited for low Reynolds number flow rate sensing, micropump flow rectification, and flow control in lab-on-a-chip devices. The valve uses coupling between fluid movement in a channel and an elastomeric column (flap) suspended in the fluid path to generate a strong anisotropic flow resistance. Soft lithography-based molding techniques were used to fabricate the valve, allowing for a low-cost, single-step fabrication process. Three valves—having heights of 25, 50, and 75 μm, respectively—were fabricated and experimentally evaluated; the best of them demonstrated a maximum fluidic diodicity of 4.6 at a Reynolds number of 12.6 and a significant diodicity of 1.6 at the low Reynolds number of 0.7. The valve's notable low Reynolds number response was realized by adopting a design methodology that balances the stiffness of the elastomer flap and adhesion forces between the flap and its seat. A pair of elastomer check valves integrated with a miniature membrane actuator demonstrated a flow rectification efficiency of 29.8%. The valve's other notable features include a wide bandwidth response, the ability to admit particles without becoming jammed, and flow rate sensing capability based on optical flap displacement measurements.

Keywords Check valve · Microfluidic diode · Flow rectification

J. Loverich (✉) · I. Kanno · H. Kotera
Department of Micro Engineering, Yoshida-Honmachi,
Sakyo-ku, 606-8501 Kyoto, Japan
e-mail: loverich@gmail.com

List of symbols

a	gap between the flap and the valve seat
b	valve seat width
c	flap clearance
δ	flap tip deflection
E	modulus of elasticity
h	channel height (depth)
I	second moment of area
l	length of the flap not in contact with the seat
L	flap length
ρ_{flap}	flap density
ρ_{fluid}	fluid density
ΔP_{block}	valve blocking pressure
ΔP_{free}	valve pressure drop in the free flow direction
ΔP_{flap}	uniform pressure difference across the flap
Q	volume flow rate
t	flap thickness
μ	mass per unit length of the flap
U	strain energy
w_1	channel width
w_2	width of channel containing flap
w_3	flap width
ω_{fluid}	first natural frequency of the flap in a fluid
ω_{free}	first natural frequency of the flap in free space
γ_s	interfacial surface energy

1 Introduction

Fundamental facets of lab-on-a-chip (LOC) that are highly relevant to the field of microfluidics include pumping, valving, and flow rate sensing (Stone et al.

2004). Research related to these topics dates back more than two decades, and a broad range of ways to measure and manipulate fluids on a microscale has been investigated (Laser and Santiago 2004; Nguyen et al. 2002). However, because it is highly desirable for LOC to be disposable, their commercial viability pivots on economic considerations (Jeon et al. 2002). This hurdle has rendered the majority of the early MEMS sensors and pumps (i.e., those fabricated using silicon-based processes) inapplicable for commercial LOC devices, thus presenting the need for new low-cost microfluidic technology, in terms of both materials and fabrication techniques.

Although there is considerable debate over which fabrication platform is best for LOC, those using polymer materials have received the most attention in recent research literature (Randall and Doyle 2005; Brenner et al. 2005). Poly(dimethylsiloxane) (PDMS) has been particularly attractive for many applications because of its unique high gas permeability, low loss tangent, low chemical reactivity (except at extreme pH levels), optical transparency (down to ~300 nm), good thermal stability, and low interfacial free energy. In addition, rapid-prototyped LOC features (such as micromixers and cell-trapping cavities) can be easily fabricated with PDMS using soft lithography-based molding techniques (Xia and Whitesides 1998).

The work in this paper seeks to further this technology by developing an innovative soft lithographically-compatible microfluidic diode that can be used for flow control, flow rate sensing, or flow rectification in membrane-based pumps. Although numerous valve designs using molded PDMS have been proposed, many require alignment and multilayer bonding, thus complicating their integration in LOC devices (Jeon et al. 2002; Unger et al. 2000; Tan et al. 2005; Yang et al. 1999). In this case, valves that can be molded in a single-step replication process are more desirable. Several fixed-geometry passive valves (i.e., nozzle-diffuser and Tesla) amenable to single-step replication have been previously described in the research literature (Gamboa et al. 2005; Tesla 1920; Anduze et al. 2001; Gerlach 1998; Xia et al. 2006). However, many of these types of valves rely on flow behavior induced by fluid inertia. For low Reynolds number (Re) flow, the nonlinear inertial term in the Navier–Stokes equation is small; therefore, the pressure drop in a fixed geometry valve is virtually invariant under flow reversal regardless of the valve's geometry (Groisman and Quake 2004). This assertion is in agreement with the experimentally measured low Re performance of diffuser and Tesla valves (Forster and Williams 2002). Clearly, different passive valve designs are required for

the low Re flows inevitable in LOC as the size of their microfluidic features approaches the nano-scale.

The valve presented in this paper uses coupling between fluid movement in a channel and a flexible column (flap) suspended in the fluid path to generate a strong direction-dependent flow resistance. Previous designs having a similar structure (fabricated using PDMS) are plagued by either poor sealing or excessive opening pressures (Adams et al. 2005; Hung et al. 2005). Recognizing that the response of these types of valves is highly dependent on the adhesion forces between elastic components in the valve, this study employed an analytical methodology to arrive at an optimum valve design free from such problems. In this pursuit, various aspects of the valve were experimentally investigated. These aspects include its scaling, dynamic performance, flow rate sensing capability, and tolerance to particle-laden flows.

2 Design and scaling

For most applications, a relevant measure of a flap valve's effectiveness is the ratio of the flow resistance for fluid moving in the direction tending to close the valve to that of flow in the opposite direction (which tends to open the valve). For clarity in this discussion, these flow directions will be referred to as "blocked" and "free," respectively. The so-called fluidic diodicity can be quantified as the ratio of the blocked (ΔP_{block}) to free (ΔP_{free}) pressure drop across the valve for a fixed flow rate Q (Gamboa et al. 2005; Gerlach 1998)
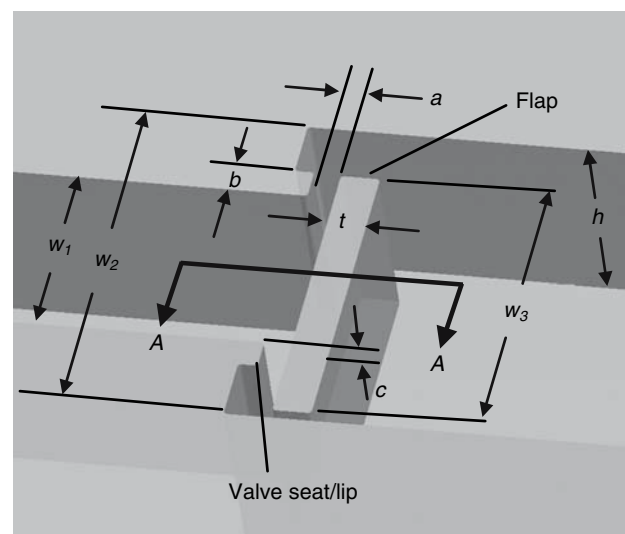

Fig. 1 Bottom view of the elastomer valve

$$\mathrm{Di} = \left(\frac{\Delta P_{block}}{\Delta P_{free}}\right)_Q. \qquad (1)$$

In general, a high valve diodicity is desirable in micropumps because it renders efficient flow rectification.

To obtain a high flap valve diodicity for low Re flow, the sensitivity of the flap deformation to changes in the flow direction should be maximized. The obvious PDMS-molded structure for realizing this objective is a thin elastomeric column suspended from the top of a wide channel and located near the mouth of a narrower channel. An illustration showing the bottom-side of this valve design is shown in Fig. 1. Depending on the flow direction, the flap either seats on the entrance of the narrow channel or opens into the wide channel.

Although the valve design is seemingly straightforward, adhesion between the PDMS flap and its seat significantly complicates its implementation. For example, after the valve is removed from the mold, small perturbations of the flap can cause it to collapse onto the valve seat and adhere closed, or stick to the top of the wide channel in an open configuration. This behavior is particularly problematic if the PDMS is treated with oxygen plasma, which can increase the interfacial free energy to 59 mJ m^{-2} (Chaudhury and Whitesides 1991). Unlike other stiction and pull-down problems in silicon MEMS devices, the adhesion of PDMS structures occurs in free space without the assistance of fluid surface tension forces.

To prevent the valve from sticking, it was designed using methods similar to those used to analyze high aspect ratio micro-contact printing stamps (Hui et al. 2002). In particular, the work required to change the strain energy in the elastomer flap must be greater than that required to change the interfacial free energy at the contacting elastomer surfaces (Sharp et al. 2004). This analysis technique can be described more precisely by considering the case when the flap has been artificially perturbed so that it is contacting the valve seat (Fig. 2). Assuming that the flap undergoes small deformation that is uniform across the valve width w_3, elementary Euler beam theory can be used to describe the flap strain energy U, giving

$$U = \frac{24EIa^2}{l^3}, \qquad (2)$$

where E is modulus of elasticity of the elastomer, I is second moment of area, a is the gap between the flap and the valve seat, and l is the length of the flap that is not in contact with the seat. If, in terms of minimizing the system's potential energy, it is more favorable for
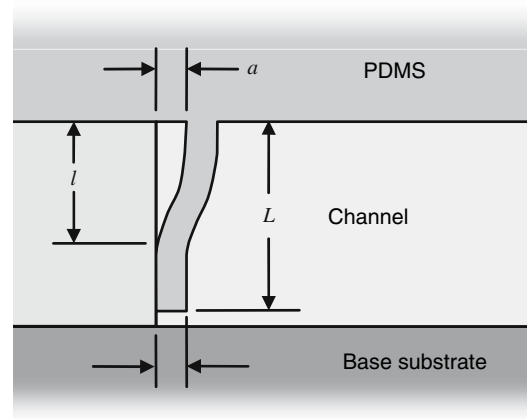

Fig. 2 Cross-section of the flap valve (Section A–A in Fig. 1)

the contact length to decrease (causing an increase in l), the strain energy will change according to

$$dU = -\frac{72EIa^2}{l^4}dl. \qquad (3)$$

The strain energy will continue to decrease as long as decreases in dU are greater than the work dW required to separate the contacting surfaces by dl. Denoting the contact width as b and the interfacial surface energy as γ_s, dW is given by

$$dW = 4b\gamma_s dl. \qquad (4)$$

Based on Eqs. 3 and 4, the flap will always completely separate from the valve seat ($l \rightarrow L$) if the following condition is met.

$$\frac{18EIa^2}{L^4\gamma_s b} > 1. \qquad (5)$$

Table 1 Valve dimensions

Valve designs	A	B	C
Channel			
w_1	25.2	51.8	76.1
w_2	50.0	100.6	150.6
h	25.5	52.3	72.8
Flap			
c	1.9	2.2	2.0
a	3.5	4.6	5.6
t	4.8	4.5	14.4
w_3	38.0	78.5	114.2
Seat			
b	3.5	6.0	8.5
Stiction criteria (Eq. 5)	1.46	1.02	1.59

Table 2 SU-8 fabrication parameters

Target thickness (µm)	2	25	50	75
SU-8 series	2,002	3,050	3,050	3,050
Spin rate (rpm)	2,000	3,800	2,050	1,350
Soft bake (min)	5	15	25	35
Exposure dose (mJ cm^2)	70	87	140	175
Post bake (min)	5	60	60	60
Development (min)	2	3	4	6
Hard bake @120°C	-	5	5	5

If the design criteria given by Eq. 5 is satisfied, the valve will not stick closed. However, this analysis does not give insight into how to design the valve such that it has a high diodicity. As mentioned previously, the diodicity will depend on how radically the flow-obstructing flap deforms in response to fluid movement. Insight into how the valve's design can be modified to enhance its diodicity can be realized by considering the flap tip deflection δ (for the free flow direction in which the flap deforms into the wide channel) for a flap width of w_3 and with a uniform pressure difference ΔP_{flap} between the up and down stream sides of the flap.

$$\delta = \frac{L^4 w_3}{8EI} \Delta P_{\text{flap}}. \tag{6}$$

The presence of the term EI/L^4 in both Eqs. 5 and 6 indicates that if the flap tip deflection is to be maximized (without risking valve stiction), one should reduce the contact width b and interfacial free energy γ_s, and increase the flap gap a and width w_3.

However, high blocked flow rates can bow a disproportionately wide flap into the narrow channel, causing back flow and leaking at the flap tip. In addition, if the overlap between the flap and its seat is not adequate, the flap will become jammed in the narrow channel. To allow sufficient overlap while minimizing

Fig. 3 Cross-section of the SU-8 valve mold

the flap-seat contact width b, a lip was added to valve seat (as shown in Fig. 1).

According to Eq. 5, wide gaps are better than narrow ones for preventing stiction. However, because large gaps cause excessive leaking near the flap root, this observation is misleading. Instead, the flap gap should be minimized while other valve parameters (i.e., flap thickness) should be adjusted to prevent valve sticking. Because the flap gap a is the smallest planar dimension in the valve, its minimum value is limited by the maximum aspect ratio that can be obtained during mold fabrication.

Adams et al. (2005) proposed a valve design that circumvented the flap leaking problems by reducing the narrow channel height compared to that of the wider channel. However, this differential height valve design was plagued by adhesion problems that rendered poor diodicity, high opening pressure (>25 kPa), and poor reliability for low Re flow. These results were confirmed in our preliminary research, leading us to abandon the differential height design in favor of the design described in this paper.

The clearance c at the flap tip is a key feature of the proposed valve design. Although flap tip clearance may not be required for high-pressure fluid flow for which the elastic PDMS channels swell, tip clearance was critical for ensuring the reliable valve operation for low Re flow considered in this paper.

Based on the described analysis, a general design procedure for elastomeric valves of this type can be ascertained: (1) choose a channel height defining the size scale of the valve, (2) select the channel and flap width (this width should be one to two times greater than the valve height, depending on the valve operation), (3) determine the minimum gap dimension, which depends on the maximum aspect ratio achievable in the mold fabrication process, (4) select a flap tip clearance (1–3 µm is sufficient for most designs with channel heights between 20 and 100 µm), and (5) adjust the flap thickness such that the stiction criteria in Eq. 5 is satisfied. The elastic modulus E of PDMS can also be modified (to satisfy Eq. 5) by adjusting the hardener concentration, but in terms of the flap stiffness, an order of magnitude reduction in the elastic modus is equivalent to halving the flap thickness (Eddington et al. 2003). Although the interfacial free energy γ_s of PDMS can also be modified to some extent with plasma and self-assembled monolayers, decreasing the interfacial free energy in microfluidic devices is sometimes undesirable because the hydrophobicity of the channel surfaces will also decrease (Xia and Whitesides 1998).
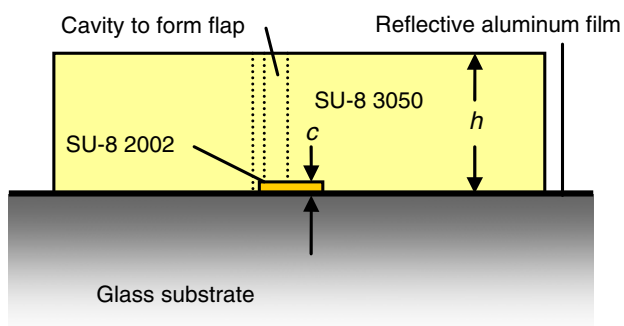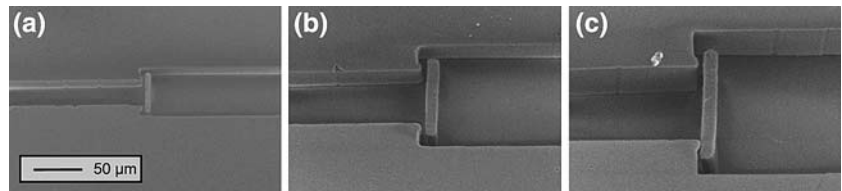
3 Fabrication

Three valves of heights 25, 50, and 75 μm, respectively, were designed according to the guidelines described in the previous section (their actual dimensions are shown in Table 1). Valve molds were fabricated using a two-step SU-8 fabrication process. An initial 2 μm thick layer provided clearance at the tip of the flap and a second, thicker layer formed the flap and fluidic channels. A standard SU-8 fabrication technique involving spin coating, soft baking, *i*-line UV exposure, post baking, developing, and hard baking was used. The recently introduced SU-8 3000 series resist was used; therefore, the optimum conditions for the fabrication are reported in Table 2. A notable adjustment in the exposure dose—compared to that typically recommended by MicroChem Corp.—was used to improve the resolution of the valve's high aspect ratio features. Reducing the exposure dose to the levels shown in Table 2 has a marked reduction in adverse affects caused by UV light diffraction about the edges of the mask and refraction at the SU-8 surface (Zhang et al. 2004). The reduced exposure dose was compensated for by increasing the post bake time to 60 min.

SU-8 master structures were used to mold the valve and channels in Sylgard™ 184 PDMS. The PDMS was prepared with a 10% by volume concentration of hardener and 80°C for 4 h curing condition, yielding a
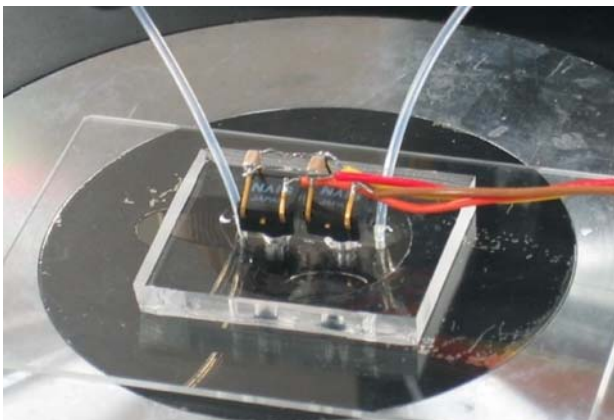

Fig. 5 Experimental apparatus for measuring the pressure drop across the valves for constant flow rates fed by a syringe pump

structure with a 1.2 MPa elastic modulus. Prior to curing, the PDMS was degassed and pins were placed into the wet PDMS to form inlet and outlet and ports for MEMS pressure sensors located on either side of each valve. Finally, the cured PDMS was treated with oxygen plasma and bonded to a glass substrate. The three different size valves are shown in Figs. 3 and 4.

4 Experiments

4.1 Diodicity

DI water was pumped through the valve at a constant flow rate using a syringe pump and the corresponding pressure drop across the valves in the blocked and free flow directions was measured using commercially available NAiS ADP5120 MEMS pressure sensors (Fig. 5). To isolate the valve resistance from that of the entrance and exit channels, an identical set of PDMS channels without flaps were fabricated and tested. The difference between the pressure drop across the flapless channel and that of those with valves is plotted versus flow rate for the three valve sizes in Fig. 6. The data shown in Fig. 6 indicates that the valves do not stick closed, even for 1.0 μl min^{-1} flow rates. The implications of this result is that the flow rate is continuous and predictable for Re approaching 0.

From Fig. 6 it is difficult to extract valuable information about how the valve will perform in flow rectification applications. A more useful measure of the valve's performance is diodicity, previously defined in Eq. 1. The non-transient valve diodicity (Di) versus Re (taken in the narrow channel) for each valve is shown in Fig. 7. The diodicity of the valve strongly depends on the flow rate. For all three valve sizes, flows having a Re less than ~0.3 are slow enough that the resulting small movement of the flap has little affect on the valve flow resistance. However, maximum diodicities of 2.7, 3.9, and 4.6 were measured at Re of 5.5, 5.4, and 12.6 for the 25, 50, and 75 μm valves, respectively. The flow rates corresponding to the valves' peak diodicities were large enough to seat the flap for the blocked flow direction and bend the flap into the open channel for flow in the opposite direction. Because high blocked-direction flow
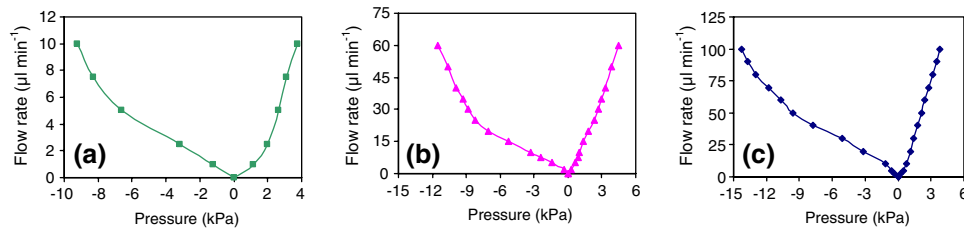
Fig. 6 Flow rate versus pressure drop across the valves for the **a** 25 μm, **b** 50 μm, and **c** 75 μm valves (positive pressures correspond to fluid moving from left to right in Fig. 4)

rates tended to fold the flap into the channel, causing excessive leaking near the tip of the flap, the diodicity decreased for high Re.

Another trend evidenced in Fig. 7 is decreasing valve diodicity with reductions in valve size. This is primarily due to fabrication-related issues. For example, high aspect ratio features were more easily fabricated in large valves than in smaller ones (aspect ratios of 13 were achieved for the 75 μm but only 7 for the 25 μm valve). Because a valve's maximum aspect ratio determines the relationship between the flap gap and height, it influences valve leaking, which in turn strongly affects the valve's diodicity. The flap tip clearance (~2 μm for all three valves) also contributed to leaking. While less tip clearance would likely improve valve diodicity, it was not pursued in these experiments due to limitations of the mask alignment method used during the UV exposure of the thick SU-8 layer. In particular, the thin 2000 series SU-8 layer (Fig. 3) was difficult to observe through the structural 3000 series SU-8 for layers thinner than ~2 μm (other alignment methods for circumnavigating this problem will be pursued in future experiments).

Nonetheless, the elastomer valve's diodicity is significant compared to other valves that can be fabricated using this low-cost and straightforward single-step replication technique (i.e., fixed-geometry Tesla
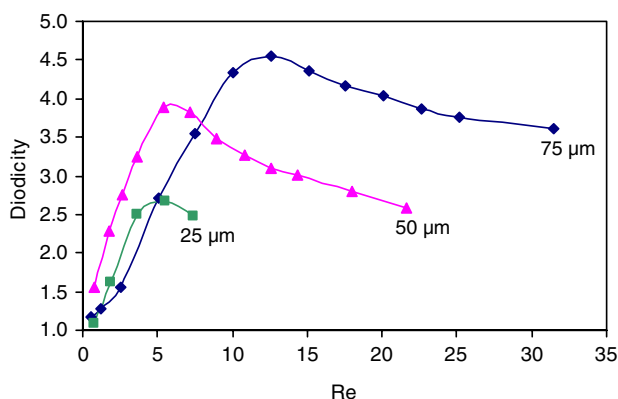
and nozzle-diffuser valves). Although nozzle-diffuser valves have been shown in the research literature to exhibit a diodicity on an order of ~1.3 for Re of 100, for Re smaller than 20 a diodicity less than 1.05 can be expected (Gamboa et al. 2005; Gerlach T 1998; Forster and Williams 2002). For low Re, the diodicity of Tesla valves is generally less than that of nozzle-diffuser valves. In this context the elastomer valve's diodicity is significant, particularly considering that the 50 μm valve demonstrated a nontrivial diodicity of 1.6 at the low Re of 0.7. Drawing a comparison with other flap-type check valves fabricated using soft elastomer materials is difficult because their response for low Re flow has been rarely reported.
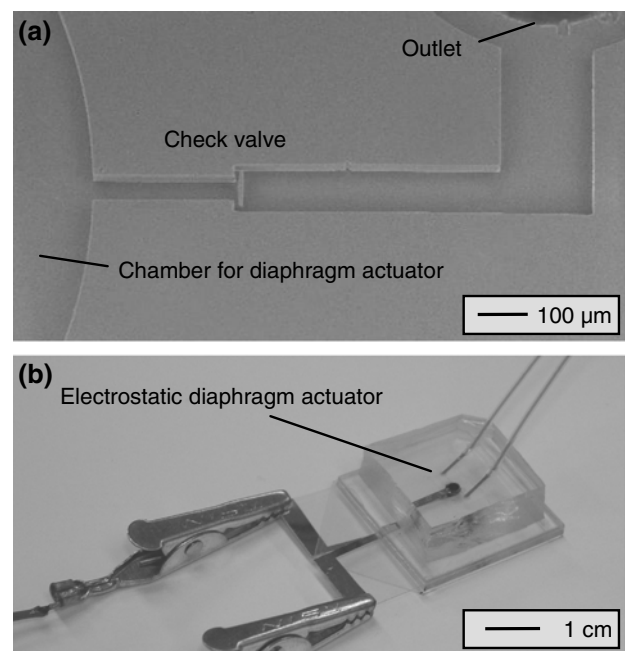

Fig. 8 a SEM image of the 50 μm microfluidic valve integrated in a micropump, and **b** an assembled micropump consisting of the elastomer valves and a dielectric elastomer diaphragm actuator
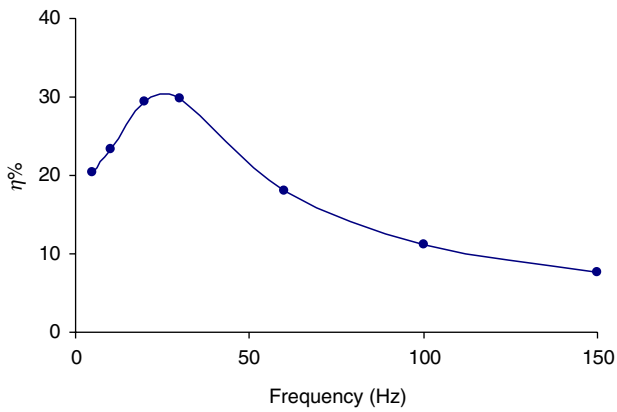

Fig. 7 Valve fluidic diodicity versus Reynolds number

Fig. 9 Flow rectification efficiency of a pair of 50 μm valves versus diaphragm actuator frequency

4.2 Dynamic response

An important implication of the valve's high diodicity for low *Re* is that efficient flow rectification can be achieved in very small micropumps fabricated using simple and low-cost techniques. In such applications, a PDMS layer containing the valves and various other fluidic components (such as inlet and outlet ports and mixing features) can be bonded directly to a substrate with a membrane actuator to pump fluid through a LOC device. One of the advantages of this micropump design is that the low-cost PDMS layer can be replaced between experimental trials to prevent sample contamination, while the more expensive actuator can be reused. This design configuration is compatible with numerous types of diaphragm components driven by electrostatic, piezoelectric, paraffin, or pneumatic actuators.

The dynamic response of the valve is important in most micropump applications, particularly if the valve exhibits resonance at frequencies lower than the fundamental natural frequency of the pump's membrane actuator. The first vibration mode of the flap that significantly influences valve operation is a cantilever beam bending mode occurring in free space at a frequency given by

$$\omega_{\text{free}} = \frac{C_1^2}{L^2} \left(\frac{EI}{\mu} \right)^{1/2} \tag{7}$$

where μ is the mass per unit length of the flap and $C_1 = 1.875104...$ (the smallest positive root of $1 + \cos C_n \cosh C_n = 0$, where $n = 1,2,3, ...$). Mass loading and damping caused by a surrounding fluid can significantly reduce the flap's resonance frequency and this effect can be accounted for by the following approximation (Sader 1998).

$$\frac{\omega_{\text{fluid}}}{\omega_{\text{free}}} = \left(1 + \frac{\pi w_3 \rho_{\text{fluid}}}{4 t \rho_{\text{flap}}} \right)^{-1/2} \tag{8}$$

ρ_{flap} is the flap density and ω_{fluid} is the resonance frequency of the flap (beam) in a fluid of density ρ_{fluid}. According to Eq. 8, the first cantilever bending mode for the 25, 50, and 75 μm valves (submerged in water) can be expected to occur at frequencies of approximately 124, 49, and 41 kHz, respectively. The upper frequency limit for which the valve can be assumed to operate quasi-statically as an inertia-less diode is somewhat less than that given by Eq. 8.

4.3 Efficiency

To experimentally investigate the valve's dynamic response, a pair of the 50 μm valves were integrated in a pump driven by a 1.5 mm in diameter dielectric elastomer actuator (Fig. 8) (Loverich et al. 2005; Pelrine et al. 1998). The flow rectification efficiency of the pair of valves was computed as the ratio of the average flow rate generated by the micropump to that which was displaced by the membrane actuator (Fig. 9). The micropump's average flow rate was measured by manually timing the rate at which a bubble traveled a fixed distance in the pump's outlet tube. The average rate at which the membrane actuator displaces fluid was estimated based on in situ membrane displacement measurements taken using a laser displacement transducer (through the transparent PDMS). The valve efficiency versus the diaphragm actuator frequency is shown in
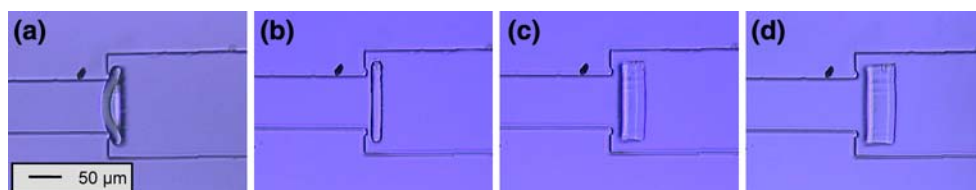

Fig. 10 Images of the 75 μm valve for flow rates of **a** 50 (in the blocked direction), **b** 0, **c** 100, and **d** 250 μl min⁻¹ (in the free direction)
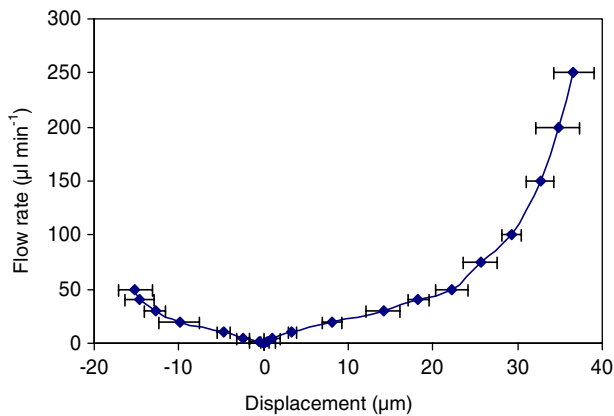
Fig. 11 Flow rate versus tip displacement for the 75 μm valve

Fig. 9. A maximum flow rectification efficiency of 29.8% was achieved at a membrane frequency of 30 Hz and pole displacement amplitude of 64.5 μm.

If the valve diodicity is assumed to be constant over the range of flow rates generated by the membrane actuator, and the pressure drop across the valve is proportional to the flow rate, the static rectification efficiency of the pair of valves can be estimated to be related to the diodicity according to $\eta = \left(\sqrt{Di} - 1\right) / \left(\sqrt{Di} + 1\right)$ (Xia et al. 2006). Considering this relationship, the valve's maximum efficiency of 29.8% would correspond to a constant diodicity of 3.4, which is close to the 3.9 maximum that was previously measured (Fig. 7). Despite the fact that the elastomer valve's diodicity strongly depends on the flow rate, the agreement between the quasi-static diodicity magnitude versus Re and the efficiency versus frequency is notable. The high frequency trend of decreasing efficiency with increasing frequency is likely due to leaking at the valve tip for the high flow rates (as was the case for the valve's diodicity versus flow rate behavior).

4.4 Flow rate sensing

Because the transparency of PDMS allows for in situ observation of the flap, the valve can be used for flow rate sensing. Top view images (Fig. 10) of the valve, captured using a digital camera and microscope, can be

digitally measured using image processing software similar to that used for particle image velocimetry (PIV). Changes in flow rate occurring slower than the reciprocal of the frequency limit given in Eq. 8 could hypothetically be resolved using this technique (>24 μs for the 75 μm valve). However, real-time flow rate measurements will likely be limited by other factors such as the imaging processing speed or the camera frame rate.

A flow rate versus tip displacement calibration curve for water flowing in the 75 μm valve (Fig. 11) was experimentally determined by feeding constant flow rates through the valve, capturing valve images, and digitally measuring the flap tip displacement. The error bars in Fig. 11 indicate the standard deviation of three sets of tip displacement measurements taken using the same valve. The sensitivity of the valve can be adjusted by changing the design of the valve in accordance with the procedure previously described in this paper.

While this flow rate sensing method requires expensive equipment and computationally demanding image processing, the sensor (valve) can be fabricated at a very low cost because it is an auxiliary feature that can be simultaneously molded with other components in the PDMS. This makes the valve sensing capability useful for application in which valves may be required and optical monitoring of the devices is possible.

4.5 Particle-laden fluids

Another useful attribute of the valve is that particles (e.g., cells) with a size on an order of that of the narrow channel can pass through unimpeded. This is possible because the valve flap is soft and elastic. In addition, these characteristics prevent the valves from damaging fragile biological matter that may be suspended in the working fluid. Images of a large fluorescent particle passing through the 50 μm valve for a constant flow rate of 40 μl min^{-1} are shown in Fig. 12. Although low volume concentrations (<0.01%) of particles were considered in this study, higher concentrations are expected to cause flow-blocking, as is the case for a fixed geometry channel having an opening with a similar size to that of the flap valve.

Fig. 12 A large fluorescent particle passing through the 50 μm valve with a flow rate of 40 μl min^{-1}

5 Conclusions

Owing primarily to factors related to cost and fabrication complexity, on-chip fluid transport and control have remained fundamental challenges in implementing lab-on-a-chip devices. The work presented herein makes strides toward addressing these issues by presenting a new microfluidic check valve that may prove to be a key component in such systems. The valve's reliable and responsive low Reynolds number characteristics make it useful for numerous applications, including flow rate sensing, flow control in microfluidic networks, and flow rectification in micropumps. Multiple valves can be molded in a single replication step, allowing for rapid low-cost fabrication. The specific set of design guidelines outlined in this paper can be used to tailor the performance and size of the check valve to optimize its performance for specific applications.

References

Adams ML, Johnston ML, Scherer A, Quake SR (2005) Polydimethylsiloxane based microfluidic diode. J Micromach Microeng 15:1517–1521

Anduze M, Colin S, Caen R, Camon H, Conedera V, Conto TD (2001) Analysis and testing of a fluidic vortex microdiode. J Micromach Microeng 11:108–112

Brenner T, Glatzel T, Zengerle R, Ducrée J (2005) Frequency-dependent transversal flow control in centrifugal microfluidics. Lab Chip 5:146–150

Chaudhury MK, Whitesides GM (1991) Direct measurement of interfacial interaction between semispherical lenses and flat sheets of poly(dimethylsiloxane) and their chemical derivatives. Langmuir 7:1013–1025

Eddington DT, Crone WC, Beebe DJ (2003) Development of process protocols to fine tune polydimethylsiloxane material properties. In: Proceedings MicroTAS. Squaw Valley, October 5–9

Forster FK, Williams BE (2002) Parametric design of fixed-geometry microvalves—the tesser valve. In: Proceedings IMECE, Paper No 33628:431–437

Gamboa AR, Morris CJ, Forster FK (2005) Improvements in fixed-valve micropump performance through shape optimization of valves. J Fluids Eng 127:339–346

Gerlach T (1998) Microdiffusers as dynamic passive valves for micropump applications. Sens Actuators A Phys 69:181–191

Groisman A, Quake SR (2004) A microfluidic rectifier: anisotropic flow resistance at low Reynolds numbers. Phys Rev Lett 92(094501):1–4

Hui CY, Jagota A, Lin YY, Kramer EJ (2002) Constraints on microcontact printing imposed by stamp deformation. Langmuir 18:1394–1407

Hung PJ, Lee PJ, Hu JC, Chen J, Rao VM, Lee LP (2005) A biomimetic elastomer check valve with diode behavior. In: Proceedings MicroTAS. Boston, October 9–13

Jeon NL, Chiu DT, Wargo CJ, Wu H, Coi IS, Anderson JR, Whitesides GM (2002) Design and fabrication of integrated passive valves and pumps for flexible polymer 3-dimensional microfluidic systems. Biomed Microdevices 4:117–121

Laser DJ, Santiago JG (2004) A review of micropumps. J Micromach Microeng 14:R35–R64

Loverich JJ, Kanno I, Kotera H (2005) A novel high energy density dielectric elastomer actuator for micro analysis systems. In: Proceedings MicroTAS. Boston, October 9–13

Nguyen N, Huang X, Chuan TK (2002) MEMS-Micropumps: a review. J Fluids Eng 124:384–392

Pelrine R, Kornbluh R, Joseph J (1998) Electrostriction of polymer dielectrics with compliant electrodes as a means for actuation. Sens Actuators A Phys 64:77–85

Randall GC, Doyle PS (2005) Permeation-driven flow in poly(dimethylsiloxane) microfluidic devices. Proc Natl Acad Sci USA 102:10813–10818

Sader JE (1998) Frequency response of cantilever beams immersed in viscous fluids with applications to the atomic force microscope. J Appl Phys 84:64–76

Sharp KG, Blackman GS, Glassmaker NJ, Jagota A, Hui C (2004) Effect of stamp deformation on the quality of microcontact printing: theory and experiment. Langmuir 20:6430–6438

Stone HA, Stroock AD, Ajdari A (2004) Engineering flows in small devices: microfluidics toward a lab-on-a-chip. Annu Rev Fluid Mech 36:381–411

Tan CKL, Tracey MC, Davis JB, Johnston ID (2005) Continuously variable mixing-ratio micromixer with elastomer valves. J Micromach Microeng 15:1885–1893

Tesla N (1920) Valvular conduit. US Patent No 1329559

Unger MA, Chou H, Thorsen T, Scherer A, Quake SR (2000) Monolithic microfabricated valves and pumps by multilayer soft lithography. Science 288:113–116

Xia Y, Whitesides GM (1998) Soft lithography. Annu Rev Mater Sci 28:153–184

Xia F, Tadigadapa S, Zhang QM (2006) Electroactive polymer based microfluidic pump. Sens Actuators A Phys 125:346–352

Yang X, Grosjean C, Tai Y (1999) Design, fabrication, and testing of micromachined silicone rubber membrane valves. J Microelectromech Syst 8:393–402

Zhang J, Chan-Park MB, Conner SR (2004) Effect of exposure dose on the replication fidelity and profile of very high aspect ratio microchannels in SU-8. Lab Chip 4:646–653